Kinetic Considerations for Strength Recovery at the Fiber–Matrix Interface Based on the Diels–Alder Reaction

Amy M. Peterson,[†] Robert E. Jensen,[‡] and Giuseppe R. Palmese*,[†]

[†]Department of Chemical & Biological Engineering, Drexel University, Philadelphia, Pennsylvania 19104, United States
[‡]U.S. Army Research Laboratory, Aberdeen Proving Ground, Maryland 21005, United States

Ⓢ Supporting Information

ABSTRACT: The Diels–Alder reaction was used to yield thermal reversibility of the bonding between a partially furan-functionalized epoxy thermosetting matrix and a maleimide-treated glass fiber. Under ambient temperature conditions, the covalent bond forming product reaction dominates, but this reaction reverses at elevated temperatures to allow for interfacial healing. Single-fiber microdroplet pull-out testing was used to characterize the coupled effects of healing temperature and the glass transition temperature (T_g) of the epoxy on interfacial strength recovery. In particular, the roles of mobility and reaction kinetics were independently varied to understand the individual effects of both.

KEYWORDS: Diels–Alder reaction, self-healing polymer, fiber-reinforced polymer composite, fiber–matrix interface, thermoset, glass transition temperature
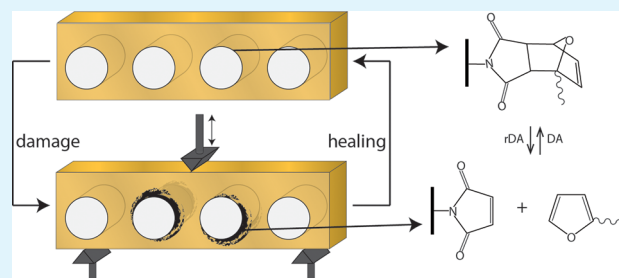
INTRODUCTION

Fiber-reinforced polymer composites are used in many applications where the need for a high strength-to-weight ratio offsets their potential for increased processing and material costs. Examples of their use can be found in the aerospace, automobile, and wind energy industries. Although fiber-reinforced composites offer superior axial strength and stiffness properties, their longer term fatigue resistance depends largely on the integrity of the bonding at the interphase region between the polymer matrix and the reinforcing fiber.[1−3] Given the mismatch in elastic moduli and coefficients of thermal expansion between the polymer matrix and fiber, the interphase region is a prime location for stress concentration and eventual crack formation under cyclic loading conditions at relatively low stresses.[4,5] Chemical and physical modifications of fiber surfaces have been shown to improve interfacial adhesion and subsequent mechanical durability.[2,3,6−8] However, in traditional fiber-reinforced composites, once fatigue damage is initiated, it is likely only to propagate.

Blaiszik et al. demonstrated fiber–polymer interfacial healing by placing resin-filled nanocapsules and catalyst (if necessary to induce polymerization) on a fiber surface.[9] Upon failure, capsules rupture and the polymer fills and cures in the crack site, resulting in recovery of 44 ± 5% in interfacial shear strength for the most effective system. Although this method demonstrates autonomic fiber–matrix crack repair, healing is limited to a single healing cycle.

Previous efforts have also shown that the functionalization of glass fibers and a polymer matrix with Diels–Alder reactive groups results in reversible bonding, and therefore healing, at the fiber–polymer interface.[10] Under ambient conditions,

furans readily react with maleimides to form adducts through the Diels–Alder reaction. At increased temperatures, adducts degrade and reform furans and maleimides. Glass surfaces were chemically treated with maleimide groups to enable the formation of covalent thermoreversible bonds with a furan-functionalized polymer network.[10] This Diels–Alder-based composite recovered 51 ± 16% interfacial shear strength. A schematic of this concept is shown in Figure 1. The Diels–Alder reaction has also be used to form recyclable[11−13] and remendable[14−19] thermosets as well as other thermally responsive materials.[20−23]

In this report, property recovery at the interface of maleimide-functionalized glass fiber and a furan-functionalized thermosetting polymer is further investigated. Of particular interest are the kinetic and physical parameters significant for Diels–Alder adduct formation. Furan concentration and polymer network glass transition temperature (T_g) were varied to evaluate the role of each on recovery of interfacial properties. Additionally, testing at increased temperatures allowed for a direct measurement of equilibrium Diels–Alder bonding at the interface.

EXPERIMENTAL SECTION

Materials. Monomers diglycidyl ether of bisphenol A (DGEBA, EPON 828, Miller-Stephenson), furfuryl glycidyl ether (FGE, Sigma-Aldrich), phenyl glycidyl ether (PGE, Sigma-Aldrich), and 4,4,′-methylene biscyclohexanamine (PACM, Air Products) were used as
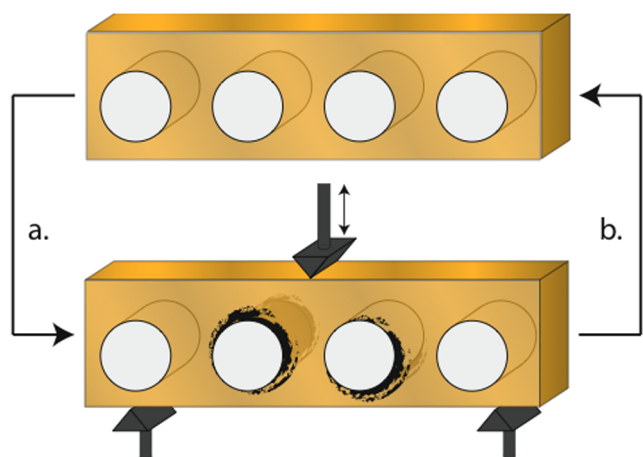
Figure 1. Schematic representation of the DA-based interfacial healing concept showing glass fibers (white) in a polymer matrix (orange). (A) Cyclic fatigue of fiber-reinforced composites leads to interfacial damage. (B) Maleimide functionalization of glass fiber within a furan-functionalized polymer network induces healing of this interface, with the potential for total property recovery.

received. Water sized E-glass fibers with an average diameter of 16 μm were kindly provided by Fiber Glass Industries, Inc. (Amsterdam, NY). Glass functionalization materials 3-aminopropyltrimethoxysilane (APS, Gelest), 1,1′-(methylenedi-4,1-phenylene)bismaleimide (BMI, Sigma-Aldrich), ethanol (Sigma-Aldrich), and N,N′-dimethylformamide (DMF, Sigma-Aldrich) were all used as received. All other chemicals were used as received from Sigma-Aldrich.

Polymer Network Preparation. Furan-functionalized thermosetting polymers were prepared as previously described.[10,18,24] Briefly, varying amounts of DGEBA, FGE, and PGE were combined and added to a stoichiometric amount of the amine curing agent PACM. The reaction scheme and structures of monomers and resulting polymer are shown in Figure 2. In the discussions that follow, in order to define the polymer networks being considered, $w_{monomer}$ represents the amount by weight of a given monomer as a fraction of all monomers bearing the epoxy group (i.e., not including the amine curing agent). For example, a polymer network containing a 6:4 weight ratio of DGEBA to FGE would have $w_{FGE} = 0.4$, $w_{DGEBA} = 0.6$, and a stoichiometric amount of PACM. Stoichiometry calculations were

carried out using EEW = 188 for DGEBA, 154 for FGE, 164 for PGE, and AHEW = 52.5 for PACM. PGE was chosen as a comonomer because it is identical to FGE except that it contains a pendant phenyl group instead of a pendant furan. By replacing some amount of FGE with a stoichiometric amount of PGE, network cross-link density could be maintained while varying furan amount. T_g values for the resulting polymer networks were characterized via differential scanning calorimetry (DSC) using a TA Instruments Q2000 at a ramp rate of 10 °C min^{-1}. DSC scans were performed over a temperature range of −50 to 200 °C with two heating/cooling cycles. T_g values were taken as the inflection point in the heat flow curve from the second heating cycle.

Glass Fiber Functionalization. Prior to use, glass fibers were cleaned in water, ethanol, and acetone to remove impurities from processing, shipping or storage. Maleimide functionalization was carried out using a two-step process as described previously.[10] First, a 1 wt % solution of APS in a 25:75 by weight ratio of ethanol and water was used to provide amine groups on the glass surface. Next, Michael Addition of malemides and amines provided maleimide functionality through the reaction of 5 wt.% BMI in DMF with surface amines. Silanation took place at 93 °C for 1 h, whereas maleimide functionalization required 2 h at 80 °C. X-ray photoelectron spectroscopy (XPS) was used to characterize the atomic composition on functionalized glass slide surfaces.

Acid-based titration was used to determine the number of amine groups per gram of amine-functionalized glass fiber. Samples were immersed in water and titrated to pH 10 with 0.05 N NaOH. Specimens were then back-titrated to pH 3 with 0.01 N HCl. The inflection point in the back-titration curve represents the point at which all amines and NaOH are consumed. Equation 1 describes the number of amine groups per gram of fiber.

$$A = \frac{V_{HCl}N_{HCl} - V_B N_B}{S} N_A \tag{1}$$

V_{HCl} is the volume of HCl, N_{HCl} is the HCl normality, V_B is the volume of NaOH, N_B is the NaOH normality, S is the fiber mass, and N_A is Avogadro's number.

Iodine titration is a technique typically used to determine the degree of unsaturation of tall oil fatty acids. ASTM D5768−02 was modified in order to use the concepts from this technique to determine the number of maleimides per gram of fiber. All modifications were performed in order to improve the sensitivity for maleimides on the fiber surface.
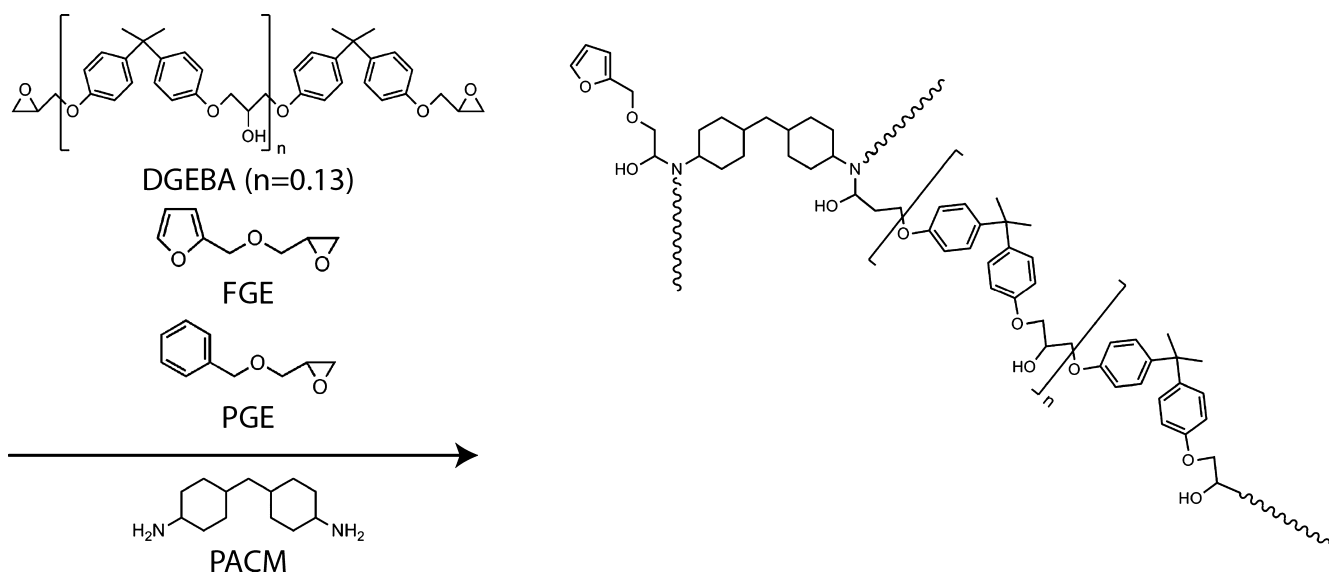

Figure 2. Structures of the monomers and resulting thermosetting polymer. The relative amounts of DGEBA and FGE are adjusted and reacted with a stoichiometric amount of the curing agent PACM in order to form polymers with different furan contents.

Fifteen g of fiber were chopped and placed in a flask. Twenty milliliters of cyclohexane and 5 mL of Wijs solution (0.1 M ICl in acetic acid) was added, and the flask was then sealed and placed in the dark for 1 h at room temperature. After 1 h in the dark, 4 mL of a potassium iodide solution (15 g of KI per 100 mL of water) and 20 mL of water were added to the flask. The contents of the flask were then titrated against 0.01 M sodium thiosulfate until the yellow color had almost disappeared; 1−2 mL of starch indicator solution (1% in water) was then added and titration continued until the blue color disappeared. Blanks containing no fiber were also run through the same procedure.

Equation 2 describes the number of maleimides per gram of fiber, M. In this expression, B is the volume of sodium thiosulfate solution required for titration of the blank, V is the volume of sodium thiosulfate solution require for titration of the specimen, N is the normality of the sodium thiosulfate solution, and S is the sample mass.

$$M = \frac{(B - V)N}{1000S} N_A \tag{2}$$

Single-Fiber Microdroplet Pull-Out Testing. The healing ability of the fiber−resin interface was investigated with single-fiber microdroplet pull-out testing.[6,10,25,26] This is a technique that has been used since the 1960s for determining interfacial properties of traditional composites containing no reversible bonds. Peterson et al. used this technique to evaluate healing efficiency by comparing delamination of virgin and healed specimens.[10]

In this procedure, a droplet of resin was cured on a single glass fiber, which was then embedded within a capillary tube, upon which a cotter pin was affixed to attached the fiber to the testing apparatus. The droplet was held static while the blades pulled down upon the microdroplet at a rate of 0.01 mm min^{-1}. Following failure, all specimens were healed and retested. Unless otherwise noted, specimens were healed for 1 h at 90 °C and 12 h at 22 °C. Increased temperature pushes the Diels−Alder reaction equilibrium toward higher reactant concentrations (greater adduct cleavage) and induces increased mobility of the network. Because the polymer used is a permanently cross-linked thermosetting material, creep of the polymer is not a concern. Instead, network mobility increases the probability that furans and maleimides will meet and potentially bond. The time at 22 °C following the increased temperature ensures that the Diels−Alder reaction equilibrium is restored to conditions that push for greater adduct formation (bonding between furans and maleimides at the interface). Additionally, this time under ambient conditions allows the polymer network to dissipate the energy added during heating, such that the properties of the polymer network before and after the healing procedure should be the same.

When testing a virgin sample, load increases with displacement up to the point of debonding, where it reaches its maximum ($F_{initial,max}$). Afterward, the droplet slides along the fiber, exhibiting a fairly constant frictional force ($F_{initial,friction}$). If a specimen is retested without healing, the load−displacement curve shows a small peak in the load that is representative of the load required to overcome static friction ($F_{no\ heal,max}$), followed by a fairly constant dynamic frictional force ($F_{no\ heal,friction}$). Following healing, specimens were tested to failure. In all cases specimens exhibited some recovery of the maximum load ($F_{healed,max}$) and comparable frictional forces to the initial and unhealed conditions ($F_{healed,friction}$). Healing efficiency was calculated according to eq 3.

$$\eta = \frac{(F_{healed,max} - F_{healed,friction}) - (F_{no\ heal,max} - F_{no\ heal,friction})}{(F_{initial,max} - F_{initial,friction}) - (F_{no\ heal,max} - F_{no\ heal,friction})} \times 100\% \tag{3}$$

This modified healing efficiency definition discounts for all frictional and inertial forces, such that any positive healing efficiency indicates recovery of properties due to the healing procedure, either through reaction of physical interactions. More extensive discussion of the testing procedure and eq 3 can be found in the literature.[10] Additionally, a series of example load−displacement curves for the

initial, no heal, and healed conditions are provided in the Supporting Information (Figure S-2).

Interfacial shear strength (IFSS) describes the quality of an interface, whether virgin or healed. In this study IFSS is used as a measure of healing. Equation 4 gives IFSS where τ_s is IFSS, d_{fiber} is the fiber diameter, and l is the embedded length of resin.

$$\tau_s = \frac{F_{healed,max}}{\pi d_{fiber} l} \tag{4}$$

Droplet diameters were limited to 150−250 μm because it was observed that healing efficiency was not dependent on droplet diameter over this range. Additionally, the ratio of the maximum load to diameter is relatively constant in this range. Prior to testing, each microdroplet was measured using an optical microscope to ensure that it fell within this range and exhibited a spherical morphology.

RESULTS AND DISCUSSION

Glass Functionalization. XPS was used to characterize glass surfaces. Atomic compositions for maleimide-functionalized glass are summarized in Table 1. A binding energy graph

Table 1. Summary of XPS Atomic Analysis Results. Values Presented Are Percent of the Total Composition

	C	O	N	Si	Na
BMI exper.	67.7	20.5	4.2	7.2	0.4
BMI theor.	68.6	20.0	8.6	2.9	0

is provided in the Supporting Information. XPS showed complete and homogeneous coverage of glass surfaces. Additionally, the experimental and theoretical values for atomic compositions are in good agreement with each other, although some impurities from the substrate (Cl, Si) are present in the spectra. Theoretical atomic compositions were calculated assuming full reaction of amines.

Although XPS provided evidence that glass was maleimide functionalized, this technique cannot provide quantitative information regarding the number of functional groups. Therefore, titration of glass fibers was used to acquire this information. Amine titration gave a surface concentration of 0.32 amines nm^{-2} for fibers after the first functionalization step, whereas iodine titration gave 0.47 maleimides nm^{-2} for fibers after the second functionalization step. Although the maleimide concentration on maleimide-functionalized fibers should be approximately the same as the amine concentration on amine-functionalized fibers, they are close and consistent with complete reaction of amines. The difference between these two values could relate to unreacted BMI adsorbed to the surface that is not removed during cleaning of the fibers. The measured maleimide surface concentration suggests that effectively no backbiting occurred on BMI-functionalized fibers.

Interfacial Healing − Role of Furan Content. The role of furan content was evaluated by adjusting w_{FGE} and w_{PGE} content while keeping w_{DGEBA} constant ($w_{DGEBA} = 0.6$). The resulting formulations were cured with a stoichiometric amount of PACM. This produced networks with constant cross-link densities, but varying amounts of furan. In this way, the role of furan concentration on healing efficiency was evaluated independent of other factors.

It was shown previously that healing efficiency is independent of furan content as long as there is furan in the network for networks of constant cross-link density.[9] However, subsequent investigation demonstrates that this behavior is only valid for $w_{FGE} > 0.1$. At $w_{FGE} = 0.05$, a healing efficiency of 16.2

817

dx.doi.org/10.1021/am302383v | ACS Appl. Mater. Interfaces 2013, 5, 815−821

± 9.2% was obtained. This deviates significantly from the healing efficiency of ~40% at w_{FGE} = 0.1 and above, as shown in Figure 3. The difference between healing efficiencies for w_{FGE} =
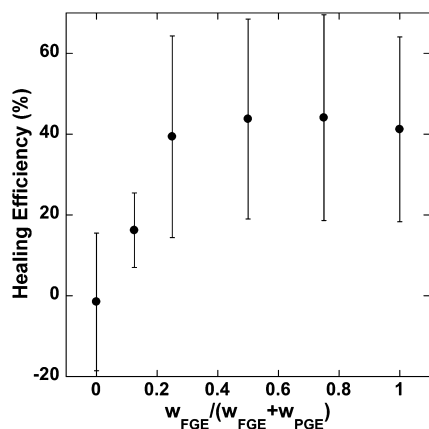

Figure 3. Effect of w_{FGE} on healing efficiency. Specimens consisted of maleimide-functionalized fibers with droplets of identical cross-link density containing varying amounts of FGE with the remainder made up of PGE. At $x = 0$, $w_{FGE} = 0$, $w_{PGE} = 0.4$ and at $x = 1$, $w_{FGE} = 0.4$, $w_{PGE} = 0$. Specimens were healed at 90 °C for 1 h and at room temperature for 12 h.

0.05 and w_{FGE} = 0.1 is statistically significant ($p = 0.021$). The null hypothesis is not rejected ($p = 0.52$) when evaluating healing efficiencies for $w_{FGE} \geq 0.1$. It is logical to conclude that the drop in healing efficiency is related to a decrease in the number of functional groups available for covalent bonding across the interface. Therefore, the minimum furan content required to achieve the maximum amount of thermoreversible bonding occurs somewhere between w_{FGE} = 0.05 and w_{FGE} = 0.1. Given the linearity of the data points for w_{FGE} = 0, 0.05, and 0.1, it is assumed that the minimum furan content to achieve optimal bonding occurs in a network with approximately w_{FGE} = 0.1.

Standard deviations for microdroplet testing are generally quite large (~20%). Scatter in the presented data is consistent with the literature and results from the nature of microdroplet testing.[27,28] The strength of the interface relates to the statistical probability that a given number of bonds will cleave under a specific force, which is complicated to replicate because eof the complexity of stresses experienced throughout the fiber, the polymer, and the interphase. The statistical nature of intimate contact during healing may compound the variability from covalent bonding, resulting in increased scatter.

Assuming that the furan concentration at the glass-polymer interface is the same as the bulk concentration, a surface concentration of 0.4 furan molecules nm^{-2} was estimated for the w_{FGE} = 0.1 formulation. This compares well with the titration-based maleimide concentration on the fiber surface of 0.47 maleimide molecules nm^{-2}. As long as $w_{FGE} \geq 0.1$, the amount of furan in the network does not affect healing efficiency and differences in healing efficiency between two networks with varying furan content result from differences in mobility, not amount of furan.

Interfacial Healing – Role of T_g. Because healing efficiency is unaffected by furan content for $w_{FGE} \geq 0.1$, healing efficiencies of networks with varying T_g values and furan contents that met this condition were evaluated simultaneously. Furan content was adjusted using w_{FGE}, whereas T_g was varied

through adjusting w_{FGE} and/or w_{PGE}. All specimens were healed for 1 h at 90 °C and 12 h at 22 °C. Results are shown in Figure 4. Healing efficiency data were plotted as a function of T_g. All
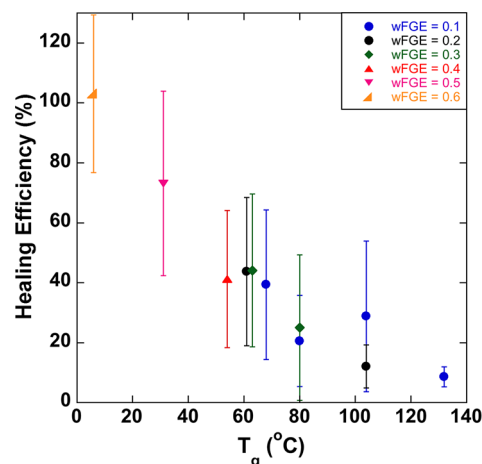

Figure 4. Effect of network T_g on healing efficiency for systems with w_{FGE} = 0.1, 0.2, 0.3., 0.4, 0.5, and 0.6 on maleimide-functionalized fibers. Different T_gs for the same w_{FGE} value were achieved by adjusting w_{PGE}. Specimens were healed at 90 °C for 1 h and at room temperature for 12 h.

points fall along a line with negative slope (R^2 = 0.89). There is a negative correlation between healing efficiency and T_g that is observed in both the raw data and the averages for each condition. The Pearson product-moment correlation coefficient for raw data is −0.584, whereas Pearson's r for the averages of all conditions is −0.932. The higher values for the raw data results in part from the greater number of data points with w_{FGE} = 0.4. At or above w_{FGE} = 0.1, healing efficiency decreases with increasing T_g (i.e., increases with increasing mobility). For example, average healing of 103 ± 26% was achieved for the w_{FGE} = 0.6 w_{DGEBA} = 0.4 system, which has a subroom temperature T_g, whereas a healing efficiency of 8.7 ± 3.7% was observed for the w_{FGE} = 0.1 w_{DGEBA} = 0.9 system (T_g = 132 °C). The relationship between healing efficiency and T_g results from the amount of time the specimen remains in a rubbery state after the adduct cleaving step (1 h at 90 °C). Mobility is necessary for bond formation because it increases the probability that a maleimide and furan will come into contact and subsequently react.

Specimens with lower T_g vitrify at a lower temperature and have more time in a mobile state. When $T > T_g$, furans have significantly more mobility and are more likely to bond with maleimides at the interface. Therefore, increasing the temperature or decreasing the T_g should both result in increased bonding at the interface. However, since furans and maleimides bond through a thermoreversible reaction, there is a competing phenomenon of decreasing equilibrium Diels−Alder adduct concentration with increased temperatures. As a result, lowering T_g is a more effective way of increasing healing efficiency.

Interfacial Healing – Role of Testing Temperature. In an attempt to characterize Diels−Alder equilibrium bond formation as a function of temperature, single-fiber micro-droplet specimens were debonded and healed according to the traditional procedure (1 h 90 °C, 12 h 22 °C), but were tested at different temperatures. Following healing, specimens equilibrated at the specified temperature for at least 1 h and

then were tested at this increased temperature. An insulated foam box was constructed around the testing stage, into which heating elements were placed. The heating elements were controlled using a benchtop temperature controller. Healing efficiency and healed IFSS for the $w_{FGE} = 0.4$, $w_{DGEBA} = 0.6$ network are shown in Figure 5 for testing temperatures ranging from 22 to 90 °C.

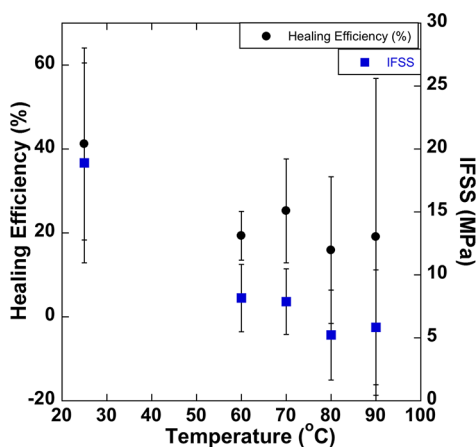**Figure 5.** Healing efficiency of $w_{FGE} = 0.4$, $w_{DGEBA} = 0.6$ microdroplets on maleimide-functionalized fibers tested at alternate temperatures. Specimens were healed for 1 h at 90 °C and 12 h at room temperature, then were equilibrated at the testing temperature for 1 h. Black circles show healing efficiencies, blue squares show IFSS values for healed specimens.

There is a temperature dependence to both healing efficiency and IFSS of the healed specimens. The Pearson product-moment correlation coefficient for the raw data is −0.604 and −0.893 for the averages of each condition. Lafont et al. also observed a temperature-dependence to healing of thermoset rubbers containing disulfide bonds.[29] Time required for full recovery of properties decreased with increasing temperature and increased with increasing T_g. Chain and network flexibility is also important in decreasing time to achieve full recovery, although the importance of mobility on recovery time becomes much less pronounced as the healing temperature increases.

To explore this behavior further, we combined the results for specimens with varied T_g values in Figure 4 with the data set of Figure 5. Healing efficiency was plotted vs $T − T_g$, where T is the testing temperature. This independent variable was selected so as to separate the effects of network properties and thermoreversible bonding. Results are given in Figure 6. Data from Figure 4 show an increase in healing efficiency with increasing $T − T_g$ (decreasing T_g); however, the specimens tested at a higher temperature display strong deviation from this behavior. The difference between the two trends can be used to determine the amount of covalent bonding as a function of temperature. Combining this with the relationship between mobility and bond formation discussed above, a model to describe bond formation at the glass−polymer interface can begin to be described.

In Figure 6, healing efficiency as a function of $T − T_g$ for networks with varying T_g values tested at room temperature follows eq 5 ($R^2 = 0.87$), the equation for the best fit line.

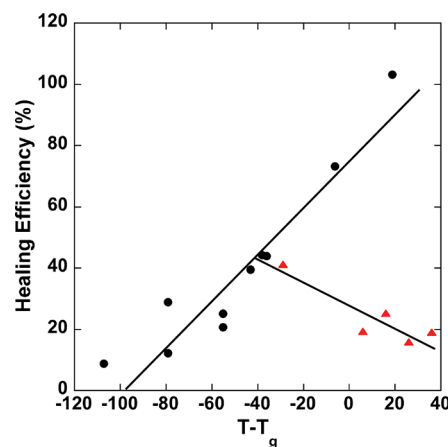$$\eta(T − T_g) = 0.7315(T − T_g) + 73.75 \tag{5}$$

Figure 6. Healing efficiency as a function of $T−T_g$ where T is the testing temperature. Black points are from Figure 4 and represent data from testing of different T_g systems at room temperature, whereas red points are from Figure 5 and represent data from $w_{FGE} = 0.4$ $w_{DGEBA} = 0.6$ specimens that were tested at increased temperatures. Lines show the best fit linear fits to the data sets.

In comparison, healing efficiency as a function of $T − T_g$ for the $w_{FGE} = 0.4$ network tested at varying temperatures, also shown in Figure 6, is described by eq 6 ($R^2 = 0.79$).

$$\eta(T − T_g) = −0.3612(T − T_g) + 28.12 \tag{6}$$

The difference between eqs 5 and 6 describes the effect of debonding at different temperatures and should result primarily from the difference in the number of adducts formed across the interface, since the effects of mobility have been taken into account by measuring healing efficiency as a function of $T − T_g$. A linear fit was chosen to describe healing efficiency at room temperature because the range of interest for equilibrium constant determination is above $T − T_g = −40$, where we see a linear relationship between healing efficiency and $T − T_g$.

Interfacial Diels−Alder Equilibrium Constant. From the difference in the slopes of the lines of eqs 5 and 6, healing efficiency decreased by 1.1% for each increase of 1 °C in testing temperature. Since the definition of healing efficiency used discounts for inertial and frictional forces, the decrease of ~1% °C^{-1} in healing efficiency corresponds to a decrease in the number of adducts across the surface of ~1% °C^{-1}. By assuming that 100% healing efficiency corresponds to complete bonding of all maleimides on the fiber surface (0.47 maleimides nm^{-2}), the relationship between temperature and adduct concentration at the interface can be described by eq 7.

$$C_A = 5.14 \times 10^{-3}(T − T_g) + 0.214 \tag{7}$$

C_A is given in number of adducts per nm^2 and T and T_g are given in K. Equation 7 is determined by taking the difference between eqs 5 and 6 and then converting healing efficiency to adduction concentration. At equilibrium, the network furan surface concentration (C_F) is the difference between the number of furans on the polymer surface and the number of adducts formed at the interface (C_A from eq 7). Similarly, fiber surface maleimide concentrations (C_M) is the difference between the surface concentration of maleimides on a fiber surface and the number of adducts formed at the interface (C_A from eq 7). With expressions for C_F and C_M, effective equilibrium constant values can be calculated as a function of temperature.

K_c, the equilibrium constant, is a measure of the relative concentration of product and reactants. However, the ability of furans to achieve equilibrium bonding based on reaction kinetics is thermodynamically limited by the mobility of furans bound to the cross-linked network, particularly when interfacial bonding is tested below or near the networks T_g. Therefore, an effective equilibrium constant, $K_{c,eff}$, that describes the actual concentrations under thermodynamically limited conditions will be determined. For the Diels−Alder reaction of furan and maleimide, $K_{c,eff}$ is defined as

$$K_{c,eff} = \frac{C_A}{C_F C_M} \tag{8}$$

Specifically, for the $w_{FGE} = 0.4$, $w_{DGEBA} = 0.6$ network and maleimide-functionalized fibers, the equilibrium constant can be described as a function of temperature:

$$K_{c,eff} = \frac{5.14 \times 10^{-3}T - 1.46}{(3.06 - 5.14 \times 10^{-3}T)(1.93 - 5.14 \times 10^{-3}T)} \tag{9}$$

The $K_{c,eff}$ values determined from eq 9 are lower than those for model (small molecule in solution) systems. For example, at 22 °C, $K_{c,eff} = 0.088$ according to eq 9, as compared to K_c values ranging from 1 to 13 for model compound formulations.[30] Although K_c and $K_{c,eff}$ values decrease with increasing temperature, $K_{c,eff}$ values for the interfacial system are systematically lower. Therefore, equilibrium concentrations of adduct and reactants at the fiber−polymer interface are governed both by stoichiometry and by mobility of reactive groups. Additionally, this behavior can be described by simple equations. Because the mobility of functional groups within a polymer network is dependent upon T_g, the number of bonds that can be formed is bounded by T as well as T_g.

CONCLUSIONS

The reversible Diels−Alder reaction between a furan-functionalized epoxy-amine thermosetting matrix with a maleimide-functionalized glass fiber was used to impart remendability at the polymer−glass interface for potential application in glass fiber-reinforced composites. It was found that mobility plays an important role in the formation of Diels−Alder adducts, as Diels−Alder bond formation is effectively halted upon vitrification of the polymer network. Complete recovery of interfacial strength was recovered for a system with $T_g = 6.1$ °C. Single-fiber microdroplet testing performed above 60 °C deviates significantly from the trend of increasing healing efficiency with increasing mobility, suggesting that Diels−Alder bonds play a major role in strength recovery at the fiber-polymer interface. Furthermore, constituitive equations were derived to describe adduct concentration at the interface and equilibrium constant values as functions of T and T_g.

ASSOCIATED CONTENT

S **Supporting Information**

Further information is available including XPS raw data, a more in-depth explanation of the single-fiber microdroplet pull-out testing procedure, and representative load−displacement curves for single-fiber microdroplet pull-out testing. This material is available free of charge via the Internet at http://pubs.acs.org.

AUTHOR INFORMATION

Corresponding Author
*E-mail: palmese@coe.drexel.edu.

Notes
The authors declare no competing financial interest.

REFERENCES

(1) Jensen, R. E.; Palmese, G. R.; McKnight, S. H. *Int. J. Adhes. Adhes.* **2006**, *26*, 103−115.
(2) Wu, H.; Dwight, D.; Huff, N. *Compos. Sci. Technol.* **1997**, *57*, 975−983.
(3) Drzal, L. T. *Mater. Sci. Eng., A* **1990**, *126*, 289−293.
(4) Brown, E. N.; White, S. R.; Sottos, N. R. *J. Mater. Sci.* **2006**, *41*, 6266−6273.
(5) Chen, B.; Dillard, D. A.; Dillard, J. G.; Clark, R. L. *Int. J. Fract.* **2002**, *114*, 167−190.
(6) Penn, L. S.; Bystry, F. A.; Marchionni, H. J. *Polym. Compos.* **1983**, *4*, 26−31.
(7) Mäder, E.; Freitag, K. H. *Composites* **1990**, *21*, 397−402.
(8) Yim, J. H. PhD Thesis, Drexel University, Philadelphia, PA, 2011.
(9) Blaiszik, B. J.; Baginska, M.; White, S. R.; Sottos, N. R. *Adv. Funct. Mater.* **2010**, *20* (20), 3547−3554.
(10) Peterson, A. M.; Jensen, R. E.; Palmese, G. R. *Compos. Sci. Technol.* **2011**, *71* (5), 586−592.
(11) Zhang, Y.; Broekhuis, A.; Picchioni, F. *Macromolecules* **2009**, *42*, 1906−1912.
(12) Watanabe, M.; Yoshie, N. *Polymer* **2006**, *47*, 4946−4952.
(13) Gandini, A. *Polym. Chem.* **2010**, *1*, 245−251.
(14) Chen, X.; Dam, M.; Ono, K.; Mal, A.; Shen, H.; Nutt, S.; Sheran, K.; Wudl, F. *Science* **2002**, *295*, 1698−1702.
(15) Bergman, S. D.; Wudl, F. *J. Mater. Chem.* **2008**, *18*, 41−62.
(16) Park, J. S.; Takahashi, K.; Guo, Z.; Wang, Y.; Bolanos, E.; Hamann-Schaffner, C.; Murphy, E.; Wudl, F.; Hahn, H. T. *J. Compos. Mater.* **2008**, *42*, 2869−2881.
(17) Adzima, B. J.; Kloxin, C. J.; Bowman, C. N. *Adv. Mater.* **2010**, *22*, 2784−2787.
(18) Peterson, A. M.; Robert E. Jensen, R. E.; Palmese, G. R. *ACS Appl. Mater. Interfaces* **2010**, *2* (4), 1141−1149.
(19) Peterson, A. M.; Robert E. Jensen, R. E.; Palmese, G. R. *ACS Appl. Mater. Interfaces* **2009**, *1* (5), 992−995.
(20) Costanzo, P.; Beyer, F. *Macromolecules* **2007**, *40*, 3996−4001.
(21) Dirlam, P. T.; Strange, G. A.; Orlicki, J. A.; Wetzel, E. D.; Costanzo, P. J. *Langmuir* **2010**, *26*, 3942−3948.
(22) Urban, M. W. *Prog. Polym. Sci.* **2009**, *34*, 679−687.
(23) Liu, Y.; Hsieh, C.-Y.; Chen, Y. *Polymer* **2006**, *47*, 2581−2586.
(24) Pratama, P. A.; Peterson, A. M.; Palmese, G. R. *Macromol. Chem. Phys.* **2011**, 1−14.
(25) Miller, B.; Gaur, U.; Hirt, D. E. *Compos. Sci. Technol.* **1991**, *42*, 207−219.
(26) Dirand, X.; Hilaire, B.; Soulier, J.; Nardin, M. *Compos. Sci. Technol.* **1996**, *56*, 533−539.
(27) Zhandarov, S.; Mäder, E. *Compos. Sci. Technol.* **2005**, *65*, 149−160.
(28) Pitkethly, M. J.; Favre, J. P.; Gaur, U.; Jakubowski, J.; Mudrich, S. F.; Caldwell, D. L.; Drzal, L. T.; Nardin, M.; Wagner, H. D.; Di Landro, L.; Hampe, A.; Armistead, J. P.; Desaeger, M.; Verpoest, I. *Compos. Sci. Technol.* **1993**, *48*, 205−214.

(29) Lafont, U.; van Zeijl, H.; van der Zwaag, S. *ACS Appl. Mater. Interfaces* **2012**, *4* (11), 6280−6288.

(30) Peterson, A. M. PhD Thesis, Drexel University, Philadelphia, PA, 2011.